8. Confocal Brightfield Imaging Techniques Using an On-Axis Scanning Optical Microscope

C. J. COGSWELL AND C. J. R. SHEPPARD

I. Introduction

Confocal microscopes have become an established tool in a wide range of professions, mostly owing to rapid commercial development of a few microscope designs optimized to image a rather narrow range of object characteristics specific to each discipline. In the fields of metallurgy, electronic device manufacture and industrial inspection, the prevalence of subjects with highly reflective surface morphologies has led to the development of confocal reflection brightfield microscopes for viewing and measuring three-dimensional surface topographies. In the bio-medical fields, the great upsurge in the use of fluorophore-conjugated antibodies to label a vast range of cell constituents has stimulated the development of commercial laser-scanning instruments optimized for the reflected fluorescence mode. These instruments, if they provide confocal reflection brightfield capabilities at all, generally perform as if the optics were added as an afterthought, with little regard for the quality of performance or for understanding and evaluating the images produced. Another class of confocal microscopes includes the real-time or tandem-scanning designs, which use Nipkow discs and incoherent light sources. Although these have been used successfully to examine biological subjects such as teeth and bone in reflection, they are more suitable for looking at highly reflecting or scattering objects because they can detect only a small fraction of the incident illumination.

In view of the fact that few commercial instruments have reflection modes which can produce high quality confocal images of weakly scattering biological subjects, we believe that there is still a great need to develop new techniques so that the full advantages of confocal microscopy can be realised. Since biologists continue to employ as standard routine a wide range of non-fluorescence conventional microscope techniques such as brightfield, phase contrast and differential interference contrast, in both transmission and reflection, we believe

CONFOCAL MICROSCOPY
ISBN 012-757270-8

that there is great potential for acquiring new information by carefully incorporating these traditional optical configurations into a confocal design. This chapter discusses some of the advantages as well as the pitfalls that may be encountered in designing and applying non-fluorescence confocal systems (henceforth referred to collectively as brightfield systems) and some of the factors to be considered in interpreting the resulting images.

II. Microscope design considerations

II.1. Choosing the optimum design configuration for brightfield optics

To start, we must consider what type of microscope design will be most appropriate to our goal of obtaining high-resolution images (in both the axial and transverse directions) in a variety of possible confocal brightfield configurations. Since many biological subjects contain only small variations in refractive index, reflection signals will often be weak, necessitating the use of some type of laser illumination. Confocal microscope designs which use laser sources fall into two categories:

(1) Off-axis beam scanning, in which some type of mirror arrangement or beam deflector is used to scan the illuminating beam through an objective and across a stationary subject [Carlsson *et al.*, 1985].

(2) On-axis specimen or objective scanning, in which the illuminating beam remains stationary on the optical axis and either the subject (on the microscope stage) or the objective is scanned [Sheppard, 1977].

Although these two designs may at first appear to be very similar in their overall imaging properties (see Chapter 3 in this volume for a more detailed description) they are not similar with respect to their overall potential for producing maximum resolution, aberration-free reflection images [Cogswell *et al.*, 1990].

A simple way of comparing the performance of the two types of instruments is to mount a front-surface mirror at the specimen plane and limit the transverse scanning pattern to a single point or line, while simultaneously changing the focus of the microscope over a precise distance (along the z-axis). Plotting the resulting signal intensity from the detector plane versus the axial position of the focus gives a method of measuring axial resolution (i.e. full width at half maximum (FWHM) measurements of the central peak) as well as a technique for detecting the presence of aberrations (i.e. deformities in the shape of the central peak and/or the presence of side-lobes). We refer to this type of measuring technique as a $V(z)$ plot. Figures 8.1 and 8.2(a) show a comparison of the performance of the same high numerical aperture (N.A.=1.4), highly corrected (planapo) objective

on both a beam-scanning and an on-axis scanning microscope. Figure 8.1(a) demonstrates the appearance of a typical x-z image of the mirror sample using a beam-scanning instrument. The beam-scanning microscope used in this example was a Bio-rad MRC-500 used in the confocal reflection mode. In this type of imaging configuration the beam is made to scan repeatedly across a single horizontal line (i.e. the y-axis position of the beam is held constant) while the focus position is stepped through several planes in the vertical z dimension. Figures 8.1(b-d) are graphs of signal intensity, I, versus position in depth (z-axis) which were created by plotting the signal strength (brightness) along a vertical line drawn through the x-z images at some chosen value of x. Figure 8.1(b) is a graph from near the centre while Figures 8.1(c) and 8.1(d) are from opposite edges of the scanned field.

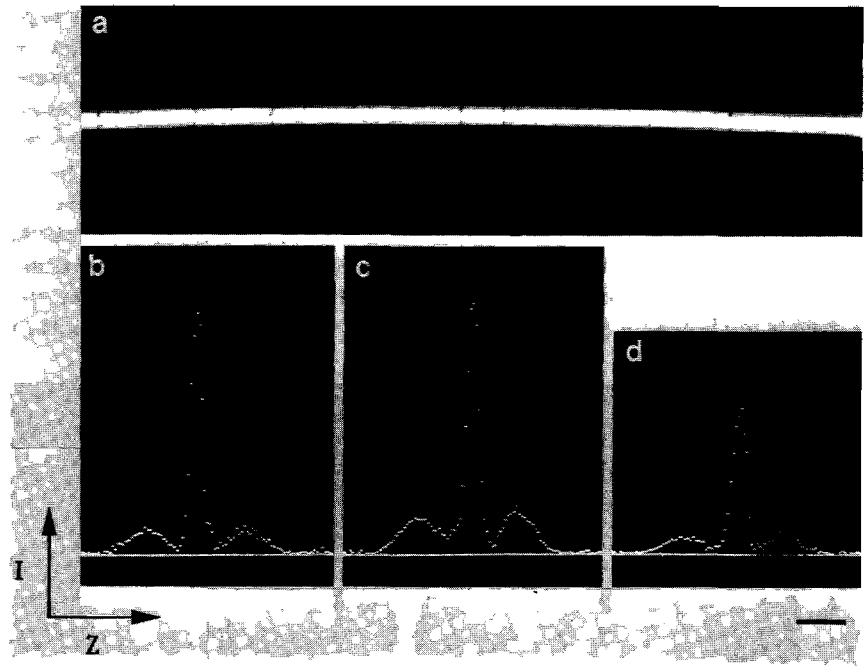

Figure 8.1. Performance of a planapochromat, N.A.=1.4 objective on an off-axis beam-scanning microscope. (a) A typical x-z image from a front-surface mirror placed at the specimen plane. In this example, $y = 255$ in vertical screen coordinates (centre of field). Dark vertical lines correspond to surface scratches on the mirror. (b) $V(z)$ plot of intensity, I, versus depth in z for $y = 255$, $x = 415$ in horizontal screen coordinates, (centre of field). (c) $V(z)$ plot for $y = 0$, $x = 735$, (top edge of field). (d) $V(z)$ plot for $y = 511$, $x = 735$, (bottom edge of field). This $V(z)$ method shows that there are variations in axial resolution (FWHM measurements of the central peak), signal intensity (height of central peak) and aberrations (shape and strength of side-lobes) as the beam scans across the field in x and y. Horizontal scale=2μm in z.

Variations in signal shape and intensity become apparent as the beam is scanned across the field in both the x and y directions. Although these variations are probably not much of a factor in obtaining usable fluorescence images (owing to the need to use larger detector pinholes and perhaps signal averaging for most biological applications) they most certainly must be considered to be an impairment to producing diffraction-limited images in brightfield reflection. One further drawback to the beam-scanning design is that to obtain medium or low magnification images a lower power (and consequently lower N.A.) objective must be utilised. This results in loss of axial (and lateral) resolution as well as increasing the likelihood that aberrations will be present.

Figure 8.2(a) is a plot of intensity versus depth in z using the same objective and mirror sample on a specimen-scanning microscope at the University of Oxford. The fairly narrow peak and small side-lobes represent good axial resolution with a minimum of aberrations, which of course will remain constant over the entire image field since the beam remains stationary on-axis. Interestingly, the peak can be made even narrower (i.e. axial resolution improved) and the side-lobes further reduced if a high numerical aperture (N.A.=1.3) fluorite (non-flat field) objective is inserted in place of the planapo lens, Figure 8.2(b). We interpret this to result from the fact that the planapochromat objective, because it is corrected for flat field, exhibits some residual aberrations on-axis. When used on the beam-scanning microscope, the fluorite objective also showed a slight improvement in resolution and a reduction

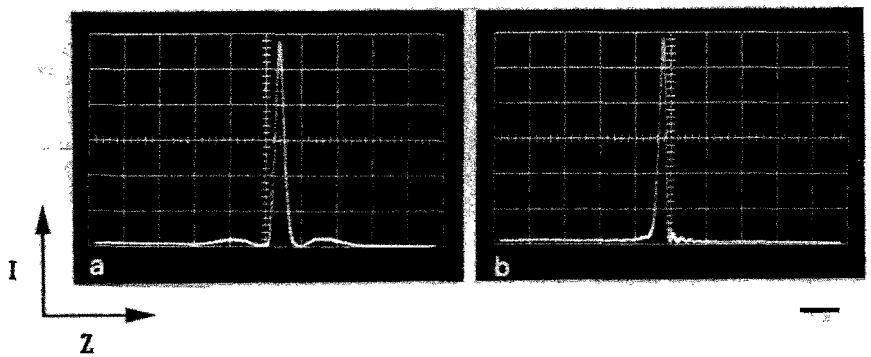

Figure 8.2. (a) $V(z)$ plot shows the performance of the same planapochromat, N.A.=1.4 objective used in Figure 8.1, but here it was tested on an on-axis specimen-scanning microscope. The narrow central peak and small side-lobes indicate good axial resolution and a minimum of aberrations which, of course, remain constant since the specimen is scanned rather than the beam. (b) $V(z)$ plot from another objective (fluorite, N.A.=1.3) used on the specimen-scanning microscope shows an improved axial response (narrower peak) and even smaller side-lobes. Horizontal scale=2μm in z.

of side-lobes when measured in the centre of the field, but this condition rapidly deteriorated as the beam scanned toward the periphery: the signal intensity became extremely variable and aberrations such as curvature of field and astigmatism were noticeably present.

Because of the difficulties inherent in the beam-scanning design, we have found it preferable to use an on-axis specimen-scanning configuration. This design eliminates the difficulty of correcting off-axis aberrations in the objective lens and has the further advantage of being able to use a single, high numerical aperture objective for the entire range of desired image magnifications; low-power imaging being achieved by simply increasing the specimen scanning distance. Still another advantage of the on-axis configuration is that a variety of brightfield techniques may be utilized which would be difficult or impossible to achieve with a beam-scanning system. Transmitted differential phase contrast, full-colour reflection, and differential interference contrast are but a few of the techniques described in this chapter which show great promise for biological imaging using a specimen-scanning confocal microscope.

II.2. Scanning speed

Before continuing this discussion, it is probably important to address what we believe to be an unfortunate misconception linked to the specimen-scanning confocal microscope — that it is too slow to be used for imaging most biological material [Inoué, 1989]. The scanning rate of our microscope makes it possible to obtain a 256 x 256 pixel image in 2.5 to 3 seconds which, interestingly, is within the range of several commercial beam-scanning instruments. As more theoretical and experimental work is published in the area of confocal fluorescence microscopy, it is becoming increasingly accepted that there is a finite limit to the speed in which a usable fluorescence image can be obtained, owing to the interplay between such factors as laser intensity versus fluorophore bleaching, detector pinhole size versus axial resolution, and detection of photons from the fluorescing sample versus background noise [Inoué, 1989]. For a full-frame image, this temporal limit may be anywhere from a very few to many tens of seconds, depending on whether the signal must be averaged over several frames. In this light, the slower maximum rate of operation of the specimen-scanning design should no longer be considered a major obstacle to most applications in biological imaging.

Another misconception linked to this microscope design is that moving the stage causes detectable vibrations in specimens composed of fresh or unfixed biological matter, making the system unusable. We have made many fresh preparations of a variety of plant cells mounted

in water with a sealed coverglass and detected no intra- or extracellular motion using our specimen-scanning microscope (for example, see Figures 8.5, 8.11, 8.13 and 8.14). However, we do not pretend to have made exhaustive studies of the suitability of this system for examining all possible types of fresh material. Certainly, as in all types of biological microscopy, there will be limitations. However, a full appreciation of the advantages and limitations of the instrumentation to be used will influence the development of techniques for optimizing sample preparation.

III. Reflected brightfield

Because of its ability to produce clear images from narrow planes of focus while at the same time eliminating out-of-focus flare, the confocal microscope is extremely well-suited to reflected brightfield applications which are normally difficult or impossible to achieve with a conventional microscope. However, the simplicity with which images can be obtained in confocal reflection should not mislead the observer into making quick and frequently erroneous conclusions about the nature of the original specimen. Just as microscopists and biologists have had to consider carefully the characteristics of the sample as well as the instrument when developing the scanning and transmission electron microscopes and, more recently, when developing fluorescent probes for the confocal fluorescence microscope, so must we consider the many variables which contribute to acquiring and correctly interpreting confocal brightfield images. In this section, we will discuss some of the more important of these variables such as the refractive index of all regions surrounding the sample, the physical characteristics of the subject with respect to how it will affect the incident laser light (i.e. Rayleigh scattering, absorption or transmission of certain wavelengths) and the quality and alignment of the optical system.

III.1. Sample characteristics

In order to demonstrate the many applications of confocal reflected brightfield microscopy in biology, it is useful to consider first the physical and optical properties of the subjects being examined. For ease of discussion, we have chosen to divide these sample characteristics into four general categories:

(1) Reflective surfaces.
(2) Refractive index boundaries within samples.
(3) Changes in absorption and reflection properties with wavelength (i.e. full-colour imaging).
(4) Sub-wavelength scattering objects.

However, it is important to keep in mind that most samples will simultaneously contain physical properties from more than one category, requiring careful analysis of all the potential optical attributes and how these interact to form a complex image.

III.1.1. Reflective surfaces

From within the broad range of biological subjects suitable for confocal reflection techniques, probably those most readily imaged and easily understood are ones with strongly reflecting surfaces that possess some sort of regular surface morphology (topography). Examples of subjects that fit this category are insect exoskeletal components, vertebrate teeth, pollen grains, seeds and the waxy cuticle layer on plant surfaces. Specimens can be prepared very simply, i.e. mounted in air with no coverglass, and viewed with high N.A. reflection objectives. Interpreting the resulting images is equally straightforward, since most or all of the detected signal can be attributed to scattering from surfaces, due to the relative non-reflectivity of the material beneath. An illustration of this type of subject can be seen in Figure 8.3 which is a series of images of a portion of a compound eye from an adult wild-type fruit fly, ***Drosophila melanogaster***. The eye was simply stuck to the surface of a slide and examined (in air) with a highly corrected reflection objective (0.85 N.A.). Figure 8.3(a) is a reflected brightfield image similar to that obtainable with a conventional microscope (i.e. no detector pinhole). Figures 8.3(b-d) show the same sample at three planes of focus, 2.5μm apart, but now with a 5μm pinhole in front of the detector to give confocal reflection images. Owing to the lack of signal from out-of-focus surfaces, these images are somewhat difficult to interpret when viewed individually. Therefore, in order to obtain a better understanding of the three-dimensional morphology, the confocal images can be combined in one of several ways. Figure 8.3(e) is an example of the auto-focus method of displaying depth information. It was created by comparing successive images from a through-focus series and storing the brightest value at each pixel position. This technique was also applied to an eye from a mutant strain of the same *Drosophila* species, illustrated in Figure 8.3(f), to show the severe irregularities in ommatidia development and the much less rounded and more ridge-like surface morphology of the entire compound eye.

Two other techniques for displaying three-dimensional information are probably worth illustrating at this point, since they are particularly applicable to surface topographic imaging. The first is the surface profile technique which encodes the position in depth of the brightest pixel from the through-focus series comparison. This depth

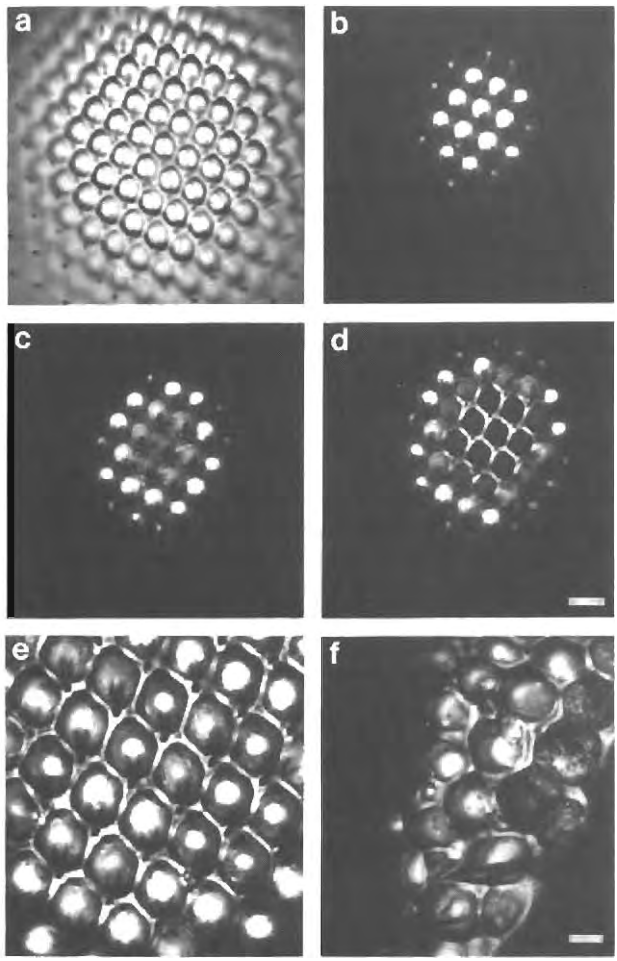

Figure 8.3. Reflection images of the compound eye of a fruit fly, *Drosophila melanogaster*, illustrate the advantages of using confocal brightfield techniques for examining biological subjects having highly reflective surface morphologies. (a) Reflected brightfield image with detector pinhole removed gives a poor axial response similar to a conventional microscope, i.e. out-of-focus planes are present in addition to the plane of focus. (b-d) A series of confocal reflection images produced by inserting a 5μm pinhole in front of the detector and changing the focus by 2.5μm intervals in depth. Now only reflections from within a very narrow plane of focus (optical section) are detected in each image. Scale=20μm. (e) Auto-focus image of a wild-type eye, created by comparing successive images from the through-focus confocal series and storing the brightest signal at each pixel position. (f) Auto-focus image of an eye from a mutant *Drosophila* illustrates an irregular, ridged morphology. Scale=10μm. Samples were stuck to the surface of a slide and examined with an N.A.=0.85 reflection objective, corrected for no coverglass.

information is displayed as a grey-level value in the resulting image, with darker grey values corresponding to signals from deeper planes of focus, Figure 8.4(b). The surface profile image can be further enhanced using pseudo-colouring routines. A second three-dimensional display method uses an auto-focus image, Figure 8.4(a), and the depth information encoded in the surface profile image to form an isometric projection, Figure 8.4(c). This technique illustrates the overall rounded surface typical of a wild-type eye as well as the regular array morphology of the ommatidia.

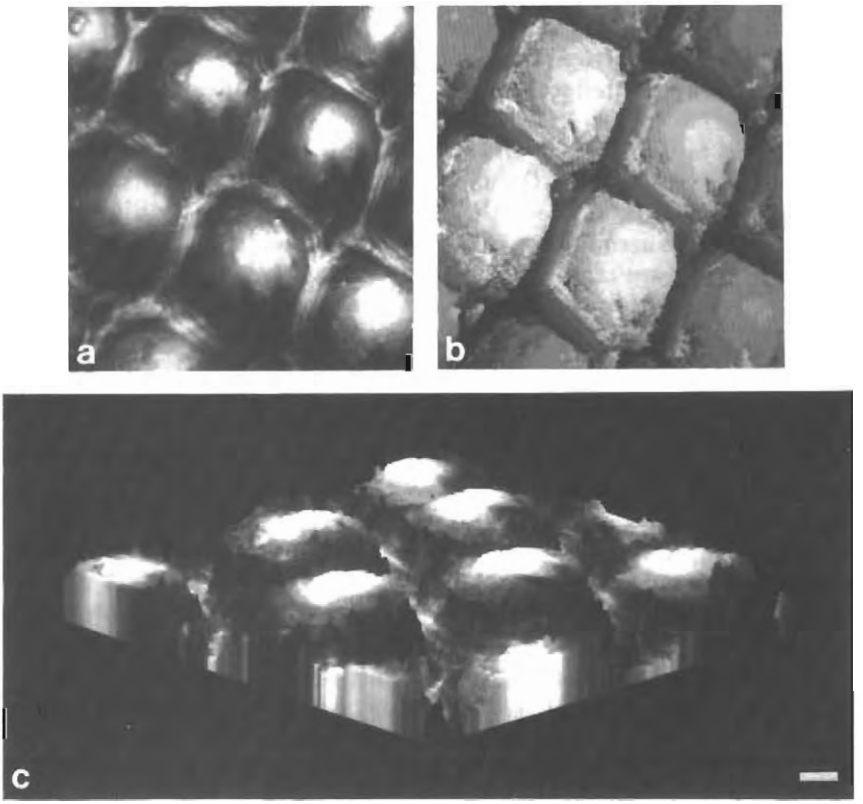

Figure 8.4. A higher magnification view of a wild-type eye of *Drosophila melanogaster* demonstrates additional techniques for displaying three-dimensional information. (a) An auto-focus image. (b) A surface profile image created at the same time as (a) but here the depth information from the focus series is represented by successively darker grey values. This creates a grey-level map of the surface morphology. (c) An isometric projection calculated from depth information in the surface profile combined with the auto-focus image. Scale=5μm.

III.1.2. Refractive index boundaries within samples

It is generally much more difficult to extract meaningful information from confocal reflection imaging techniques when the regions of interest are contained within a semi-transparent sample. This is true of a large number of biological preparations such as living whole mounts or cultures, fixed and embedded tissues, and cell or chromosome squashes. These subjects are usually placed on a microscope slide in some kind of fluid medium with an overlaying coverglass. Each of these more or less horizontal refractive index boundaries will reflect a portion of the incident light depending on such factors as angle of incidence, orientation (or tilt) of the boundary with respect to the optic axis, and the actual difference between the two refractive indices. Even when oil immersion objectives are used to match closely the refractive indices of the lens elements and coverglass, there is some loss of illumination from reflections before the initial plane of the specimen is reached.

An even more complex situation usually arises when focusing on the external boundary of the biological specimen. Strong reflections will occur at this interface if the refractive index of the object is different from the surrounding mounting or embedding medium. If the biological structure is a cell wall or membrane, then it probably will have a different refractive index from the underlying cytoplasm, and thus it will produce still another reflecting boundary (dependent on orientation as before) when this plane of focus is reached. The pattern of reflections from refractive index (phase) boundaries will continue throughout the entire focus series, with strong phase steps producing the brightest signals. Figures 8.5(a-d) illustrate this phenomenon using a fresh leaf peel from the monocot, *Rhoeo spathacea*. The tissue was mounted in water under a sealed coverglass and viewed with an oil immersion, N.A.=1.4, objective lens. The extremely bright (white) regions in Figure 8.5(a) are reflections from the waxy cuticle layer of the leaf surface, which forms a strong refractive index boundary with the underlying cells. The signal from these regions is saturated because the overall gain of the system has been increased in order to image the much weaker phase boundaries within the underlying stomatal structure. Focusing down into the specimen at 2μm intervals, Figures 8.5(a-d), shows that stomatal guard cells containing chloroplasts and accessory cells containing pigment granules have enough variations in refractive index to produce weak but easily detectable signals in confocal reflected brightfield, provided they are far enough below the cuticle layer boundary so as not to be overpowered by reflections from its plane of focus. This masking by highly refractive regions is, of course, the reason why it is extremely difficult to use reflection brightfield techniques to view biological specimens with a conventional microscope.

When imaging biological subjects of this type, further complicating factors must also be taken into account, including refraction or attenuation of the illuminating rays by inclusions in the sample such as lipid globules or opaque bodies, and interference fringes due to narrow layers of differing refractive index. These sorts of effects frequently make it extremely difficult to interpret images from complex biological structures obtained from planes of focus more than a few microns in depth below the top of the subject.

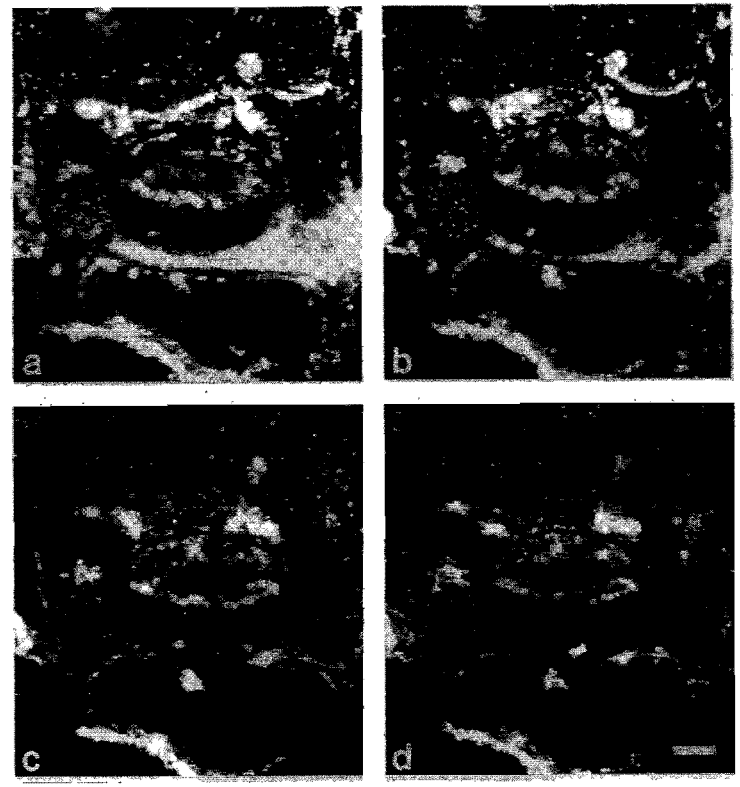

Figure 8.5. Advantages of using confocal reflected brightfield techniques for imaging refractive index boundaries within biological samples. (a-d) A series of images from a fresh leaf peel of *Rhoeo spathacea* at 2μm focus intervals. A stoma with its two half-moon shaped guard cells is seen in the centre of the field. The gain of the system was increased to allow viewing of the weakly reflecting stomatal structures. Thus, the signal saturated when focusing on the plane of the highly reflective waxy cuticle layer boundary, visible as a large white patch in (a). The optical sectioning capability of the confocal microscope makes it possible to selectively adjust the sensitivity of the system in order to detect weakly reflecting structures (provided they are not so close to a strong phase boundary as to be masked by its bright signal). Scale=15μm.

conventional microscope.

When imaging biological subjects of this type, further complicating factors must also be taken into account, including refraction or attenuation of the illuminating rays by inclusions in the sample such as lipid globules or opaque bodies, and interference fringes due to narrow layers of differing refractive index. These sorts of effects frequently make it extremely difficult to interpret images from complex biological structures obtained from planes of focus more than a few microns in depth below the top of the subject.

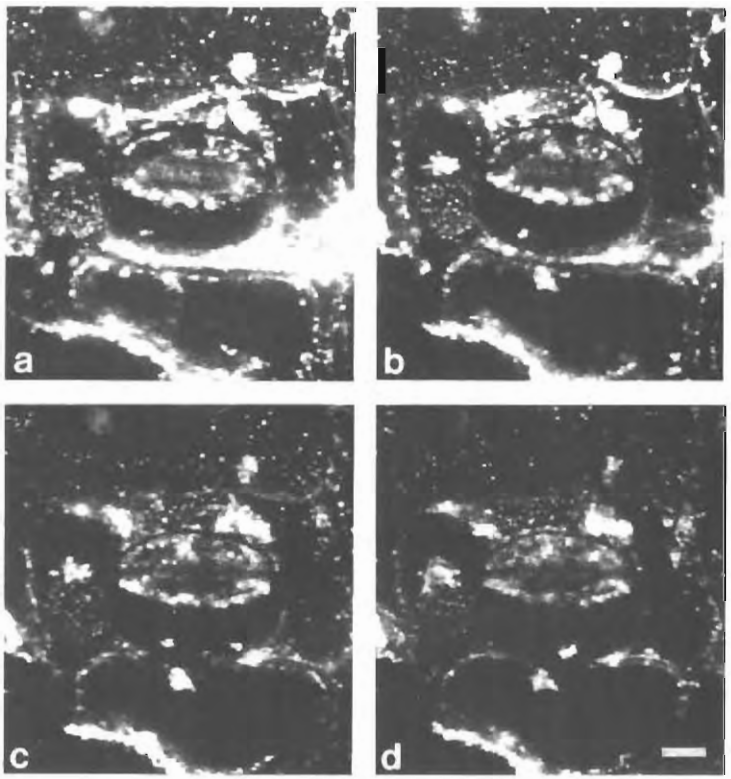

Figure 8.5. Advantages of using confocal reflected brightfield techniques for imaging refractive index boundaries within biological samples. (a-d) A series of images from a fresh leaf peel of *Rhoeo spathacea* at 2μm focus intervals. A stoma with its two half-moon shaped guard cells is seen in the centre of the field. The gain of the system was increased to allow viewing of the weakly reflecting stomatal structures. Thus, the signal saturated when focusing on the plane of the highly reflective waxy cuticle layer boundary, visible as a large white patch in (a). The optical sectioning capability of the confocal microscope makes it possible to selectively adjust the sensitivity of the system in order to detect weakly reflecting structures (provided they are not so close to a strong phase boundary as to be masked by its bright signal). Scale=15μm.

III.1.3. Changes in absorption and reflection properties with wavelength: full-colour reflected brightfield imaging

In addition to producing reflections at phase boundaries, biological structures may contain natural pigments or artificial stains which cause these reflections to vary in intensity depending on the wavelength of the illuminating source. For more than a century, coloured biological stains have been used in conventional light microscopy to enhance visibility and aid in identifying tissue sub-structure and cell constituents. We believe the ability to image colour information in biological microscopy to be such an important tool that it should be made available in contemporary confocal brightfield microscope systems.

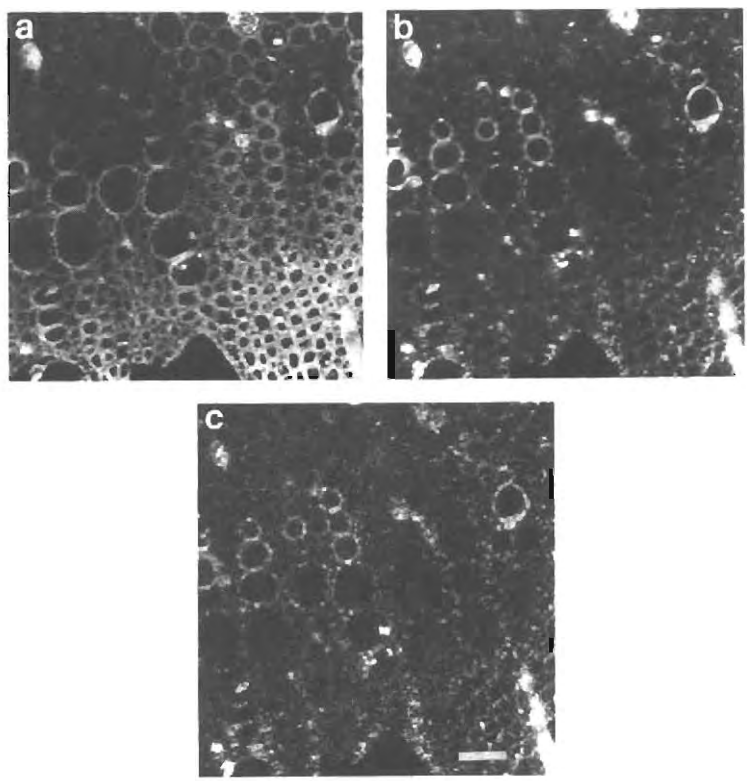

Figure 8.6. Confocal reflected brightfield techniques using red, green and blue lasers to detect differentially-stained tissue. Subject is a cross-section from a woody plant stem, *Chodanthus puberulus*, stained with alcian blue and safranin. The three images simultaneously produced with the (a) HeNe (red) laser, (b) frequency-doubled YAG (green) laser, and (c) HeCd (blue) laser can be combined to form a full-colour image. Scale=20μm.

III.1.3. Changes in absorption and reflection properties with wavelength: full-colour reflected brightfield imaging

In addition to producing reflections at phase boundaries, biological structures may contain natural pigments or artificial stains which cause these reflections to vary in intensity depending on the wavelength of the illuminating source. For more than a century, coloured biological stains have been used in conventional light microscopy to enhance visibility and aid in identifying tissue sub-structure and cell constituents. We believe the ability to image colour information in biological microscopy to be such an important tool that it should be made available in contemporary confocal brightfield microscope systems.

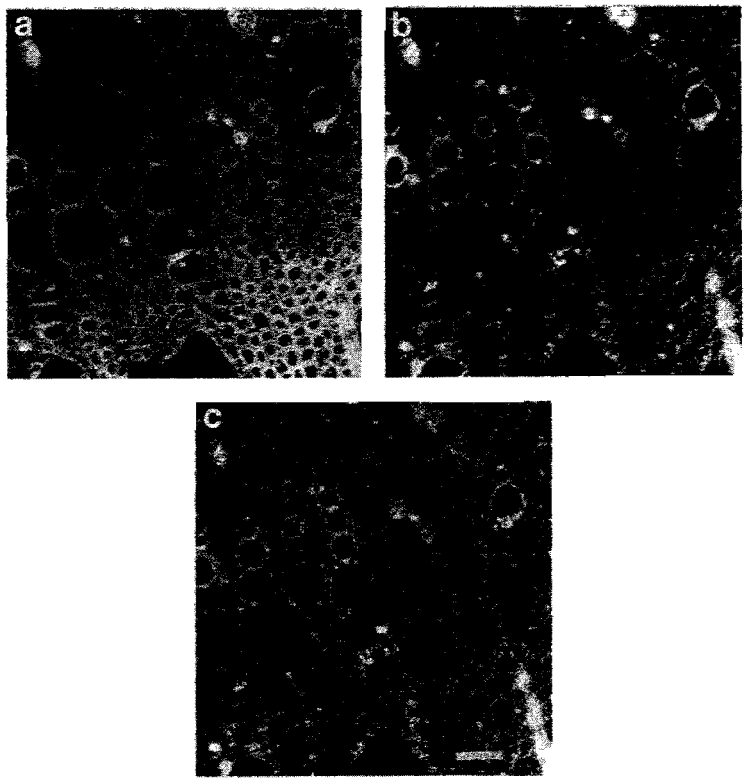

Figure 8.6. Confocal reflected brightfield techniques using red, green and blue lasers to detect differentially-stained tissue. Subject is a cross-section from a woody plant stem, *Chodanthus puberulus*, stained with alcian blue and safranin. The three images simultaneously produced with the (a) HeNe (red) laser, (b) frequency-doubled YAG (green) laser, and (c) HeCd (blue) laser can be combined to form a full-colour image. Scale=20μm.

To obtain full-colour reflected confocal images with our on-axis design, we have incorporated three lasers into our system (HeNe: 633nm; frequency-doubled YAG: 532nm; HeCd: 442nm) and simultaneously detected their signals using three separate photomultipliers. This technique can be performed more easily using apochromatic or fluorite objectives to reduce chromatic aberration effects. It also requires careful axial and transverse positioning of the three pairs of incident and detector pinholes (one confocal pair for each laser) to ensure precise registration of the resulting images. This requirement is much more easily attained with an on-axis scanning microscope, since off-axis lens aberrations, which will usually vary for different wavelengths, need not be considered. Figure 8.6 shows three reflected brightfield images of a cross-section from a woody plant stem, *Chodanthus puberulus*, fixed, embedded and subsequently stained with alcian blue and safranin. Figure 8.6(a) was made using the red HeNe laser, Figure 8.6(b) with the frequency-doubled YAG (green) laser and Figure 8.6(c) with the HeCd (blue) laser. All three images were produced at the same time and were also displayed in the red, green and blue channels of a colour monitor to produce a full-colour representation. This technique shows clearly the variations in reflectivity versus wavelength of the differently stained cell walls.

III.1.4. Sub-wavelength scattering objects

Biological samples may contain sub-structures which fall into the general category of isolated, sub-wavelength diameter particles which act as purely scattering objects. Prime examples of this type of subject are colloidal gold particles of only a few nanometers diameter, which are commonly used to label specific antibody probes for immunocytochemical experiments. The confocal reflected brightfield microscope is especially well-suited for detecting and locating (in three dimensions) these immunogold probes. However, in order to draw accurate conclusions from confocal reflection images of immunogold-labelled preparations, it is imperative to provide non-labelled control samples for comparison imaging. An example of the difficulties that can occur while imaging these gold probes is a comparison study of the plaques associated with Alzheimer's disease in human brain sections, which was recently performed in our laboratory (unpublished results). In this study we observed three serial sections: one which had been labelled with an appropriate plaque antibody linked to 1nm gold, a second which was the same as the first except that, in addition, the gold had been silver-enhanced to produce particles greater than 50nm in diameter, and a third which had been treated with 1nm gold but no antibody. Even though the label in the section containing silver-

enhanced gold was clearly visible in transmission using a conventional brightfield microscope while the other two were not, when viewed with the confocal reflection brightfield microscope all three appeared the same (i.e. plaque-like regions contained brightly reflecting particles in all three sections)! Clearly, small phase objects occurring naturally in the tissue or resulting from preparation techniques were producing reflection signals that were so bright as to overpower any signal that might have been present from the gold-labelled probe.

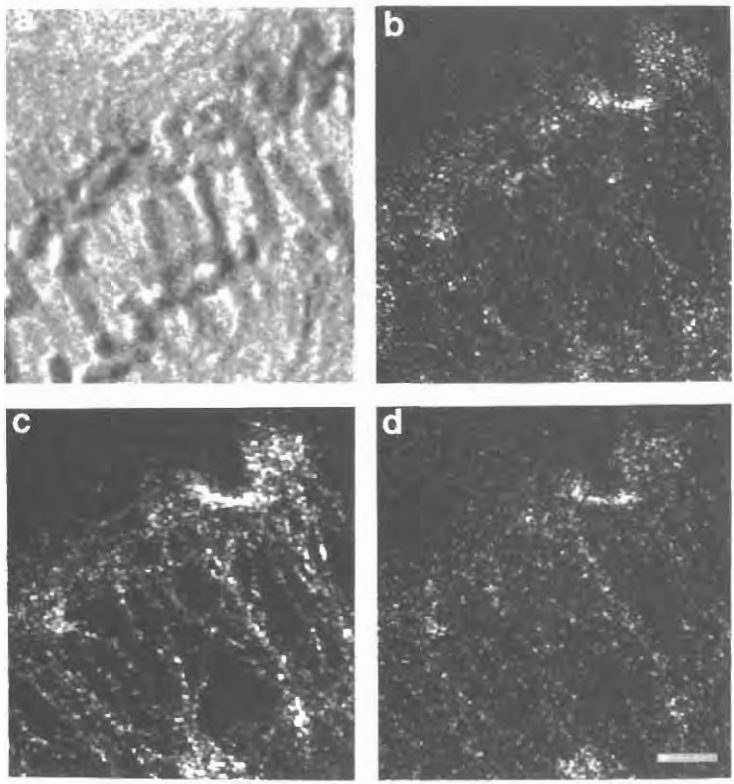

Figure 8.7. Response of sub-wavelength gold particles to confocal reflected brightfield techniques using red, green and blue laser light. Subject is an anaphase from the endosperm of an African blood lily, *Haemanthus katherinae*, which has microtubule bundles labelled with 15nm immunogold. (a) Transmitted differential phase contrast image (non-confocal), included here for reference, to show the location of the chromosomes within the microtubule bundles which comprise the mitotic spindle. (b-d) Confocal reflected brightfield images of the microtubule bundles in the same sample region using (b) HeNe (red), (c) YAG (green), and (d) HeCd (blue) lasers. The image produced with the green laser (c) shows the brightest signal which is characteristic of Rayleigh scattering by sub-wavelength gold particles. Scale=5μm. (*Haemanthus* preparations courtesy of Dr. J. Molé-Bajer and Dr. A.S. Bajer, University of Oregon.)

enhanced gold was clearly visible in transmission using a conventional brightfield microscope while the other two were not, when viewed with the confocal reflection brightfield microscope all three appeared the same (i.e. plaque-like regions contained brightly reflecting particles in all three sections)! Clearly, small phase objects occurring naturally in the tissue or resulting from preparation techniques were producing reflection signals that were so bright as to overpower any signal that might have been present from the gold-labelled probe.

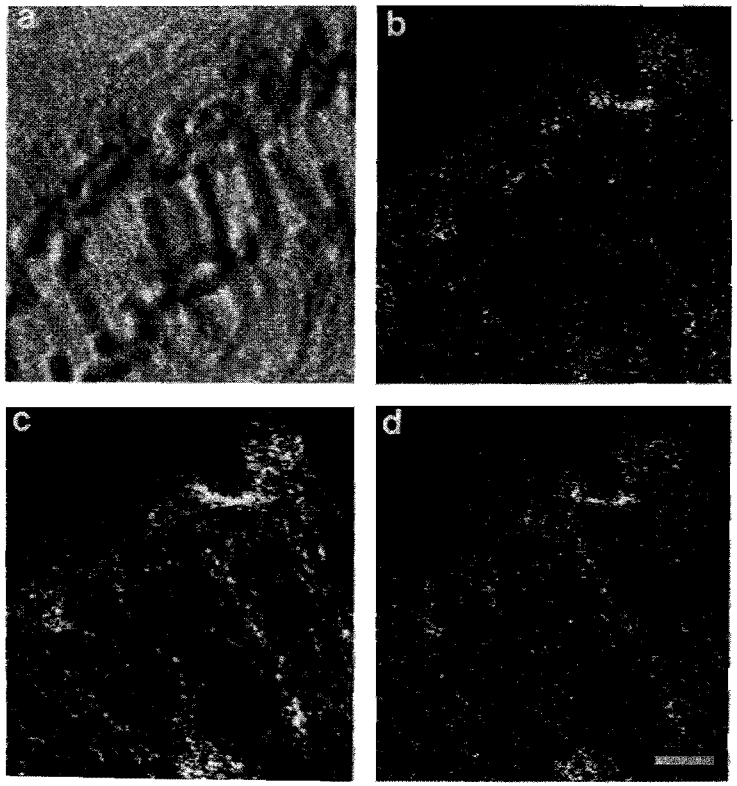

Figure 8.7. Response of sub-wavelength gold particles to confocal reflected brightfield techniques using red, green and blue laser light. Subject is an anaphase from the endosperm of an African blood lily, *Haemanthus katherinae*, which has microtubule bundles labelled with 15nm immunogold. (a) Transmitted differential phase contrast image (non-confocal), included here for reference, to show the location of the chromosomes within the microtubule bundles which comprise the mitotic spindle. (b-d) Confocal reflected brightfield images of the microtubule bundles in the same sample region using (b) HeNe (red), (c) YAG (green), and (d) HeCd (blue) lasers. The image produced with the green laser (c) shows the brightest signal which is characteristic of Rayleigh scattering by sub-wavelength gold particles. Scale=5μm. (*Haemanthus* preparations courtesy of Dr. J. Molé-Bajer and Dr. A.S. Bajer, University of Oregon.)

Sub-wavelength diameter gold particles exhibit another optical feature which is potentially useful when analysing images for the presence of immunogold labelling. Unlike silver particles, the resonance properties of gold molecules cause them to scatter green wavelengths more strongly than red or blue [Born and Wolf, 1980]. (This should not be confused with the optical behaviour of thin gold films in reflection which appear pink to red in colour.) Figures 8.7(b-d) show three images simultaneously produced using red, green and blue light, of a mitotic endosperm nucleus in the African blood lily, *Haemanthus*, in which microtubules were labelled with a tubulin antibody linked to 15nm gold. The microtubules in the image made with the green laser, Figure 8.7(c), are the brightest and most clearly delineated. This green peak response is to be expected from the Rayleigh scattering properties of sub-wavelength gold particles. (In this experiment a control specimen containing no tubulin antibody was examined and no microtubules were visible.)

These types of subjects are also well-suited to three-dimensional reconstruction and display techniques such as computer-generated stereo pairs.

III.2. Improving visual quality and resolution

In addition to carefully evaluating the physical and optical properties of the biological specimens to be examined with the confocal brightfield microscope, it is equally important to align and manipulate the instrument itself in order to obtain images with high visual quality and maximum resolution. For example, inserting additional optical elements or reconfiguring existing components in the microscope may lead to considerable improvements in the final image. In particular, we will consider three areas where careful adjustments to the on-axis design could prove beneficial:

(1) Correcting lens aberrations.

(2) Adjusting the detector pinhole size to obtain maximum lateral resolution with minimum noise.

(3) Using detector arrays to further increase resolution.

III.2.1. Correcting lens aberrations

Assuming that the user can identify by conventional means certain features of the preparation to be viewed (such as coverglass thickness, mounting/embedding medium refractive index and approximate sample thickness), it is then possible to minimize optical aberrations in the microscope if one has an understanding of how the objectives and optical elements in the system behave under controlled test con-

ditions. For example, the $V(z)$ technique described earlier in this chapter can be used to test the performance of a specific objective when the mirror reflector used as the test object has been modified with various thickness coverglasses and mounting media. For each of these known test samples, weak spherical or cylindrical correction lenses (< 1 dioptre) can be added to the beam path (before the rear pupil of the objective) to correct for any residual effects which commonly occur, such as spherical aberration and astigmatism. Figures 8.8(a-d) illustrate the effects that varying the coverglass thickness can have on the axial resolution of an objective and also the improvements that can be realized when correction lenses are inserted in the beam path. Figure 8.8(a) is a $V(z)$ plot of the signal from a mirror sample that has had a number 1.5 coverglass (0.17mm thick) mounted to its surface with a thin layer of immersion oil. The objective used in

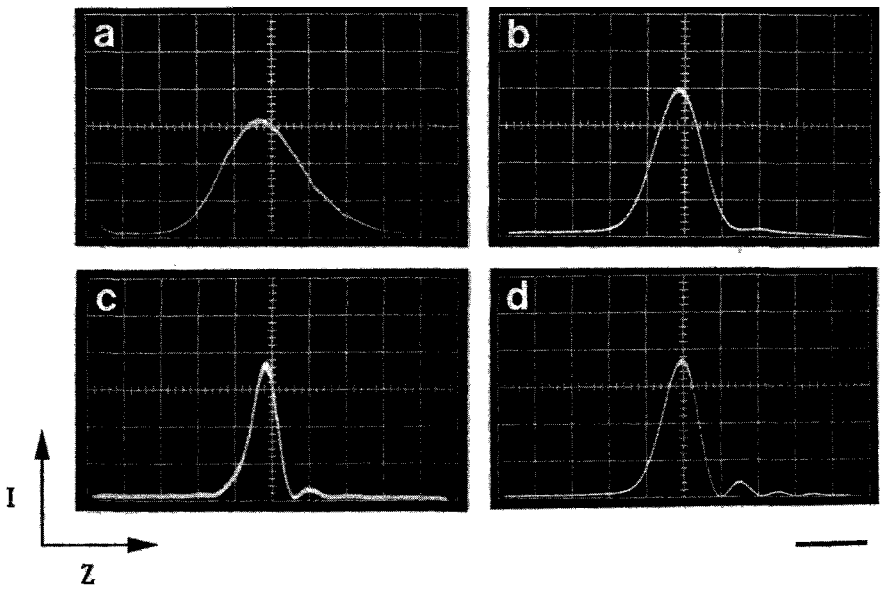

Figure 8.8. Changes in axial resolution produced by varying coverglass thickness or by inserting weakly correcting spherical lenses into the beam path. (a-d) $V(z)$ plots using an infinity-corrected, planapochromat, N.A.=1.4 objective and a mirror sample. (a) $V(z)$ plot resulting from mounting a number 1.5 coverglass (0.17mm thick) to the mirror surface with a thin layer of immersion oil. (b) $V(z)$ plot showing improvements in signal strength and axial resolution, using the same sample as in (a), produced by inserting a -0.25 dioptre spherical lens into the beam path to correct for aberrations. (c) $V(z)$ plot from a number 1 coverglass (0.14mm thick) immersed to the mirror and corrected with the same weak spherical lens. (d) $V(z)$ plot using the same correcting lens but no coverglass on the mirror. Scale=14μm in z.

this figure was an infinity-corrected planapochromat, N.A.=1.4. Figure 8.8(b) illustrates how the amplitude of the signal can be increased and the full width at half maximum (FWHM) dimension of the peak intensity improved (narrowed) when a weak spherical correction lens (-0.25 dioptre) is inserted into the beam path. Figures 8.8(c) and 8.8(d) show the best response we were able to obtain using correction lenses when the mirror had a number 1 (0.14mm thick) coverglass and no coverglass respectively. Clearly, for this particular objective and mounting medium, the best axial resolution and signal strength is obtainable with a number 1 coverglass appropriately corrected.

In order to minimize aberrations when looking at an actual biological specimen, it is of course necessary to use an objective of the correct tube length and, ideally, one that can be internally corrected for coverglass thickness as well. Even then, the fact that the system is focused through different types and thicknesses of mounting medium needs to be considered. It may ultimately prove desirable to mount some kind of reflective foil or evaporated metal film onto the microscope slide adjacent to the biological specimen so that a $V(z)$ test might first be performed on a known reflecting object which has, as nearly as possible, the same external optical properties (coverglass, mounting medium, etc.) as the biological subject. While conducting such a test, further correcting lenses could easily be added to the optical system.

III.2.2. Adjusting pinhole size to obtain maximum lateral resolution

An often overlooked feature of scanning optical microscope systems which utilize coherent light is their ability to improve lateral resolution (in the x-y plane) as well as resolution in depth [Sheppard and Choudhury, 1977]. This is because the object is effectively imaged using both incident and collected light, and may provide as much as 1.4 times the lateral resolution of a conventional microscope. Besides being adversely affected by aberrations, resolution is dependent on pinhole size and critically dependent on alignment of the pinhole on the optic axis, both in the axial (along the z-axis) and transverse directions.

To illustrate factors that improve lateral resolution in our reflected confocal brightfield design, a region out of the centre of a late mitotic anaphase nucleus in endosperm tissue of the African globe (blood) lily, *Haemanthus katherinae*, was imaged at 9,000 diameters magnification. The microtubule bundles have been labelled with 15nm immunogold. Figure 8.9(a) shows a few of these microtubule bundles imaged with a fluorite 100X, 1.3 N.A., oil immersion lens and a

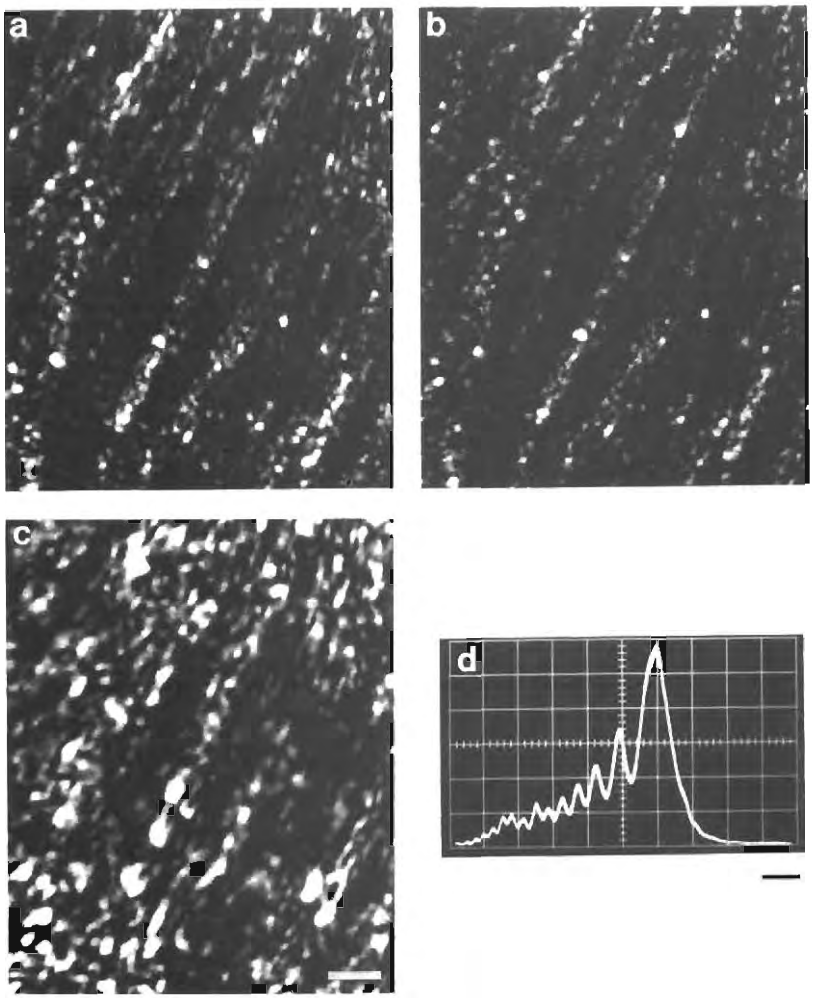

Figure 8.9. Changes in transverse resolution produced by varying the detector pinhole diameter or by introducing aberrations into the system. (a-c) Enlarged view of *Haemanthus* 15nm immunogold-labelled microtubule bundles using confocal reflected brightfield optics and a fluorite, N.A.=1.3 objective. (a) A 10 micron pinhole was placed in front of the detector. (b) Changing to a 2.5 micron detector pinhole shows an improvement in lateral resolution. Meaningful comparisons were made possible by measuring the background density and holding it constant during all steps in the photographic process. (c) Image of the same region using the same objective with its tube length correcting lens removed, i.e. the image plane (detector) is much farther away than the 160mm optimum tube length. Aberrations present in this configuration greatly reduce resolution. (d) $V(z)$ plot of this incorrect tube length condition in which side-lobes on the left side of the central peak result from spherical aberration effects of high numerical aperture. (a-c) Scale=2μm. (d) Horizontal scale=2μm in z.

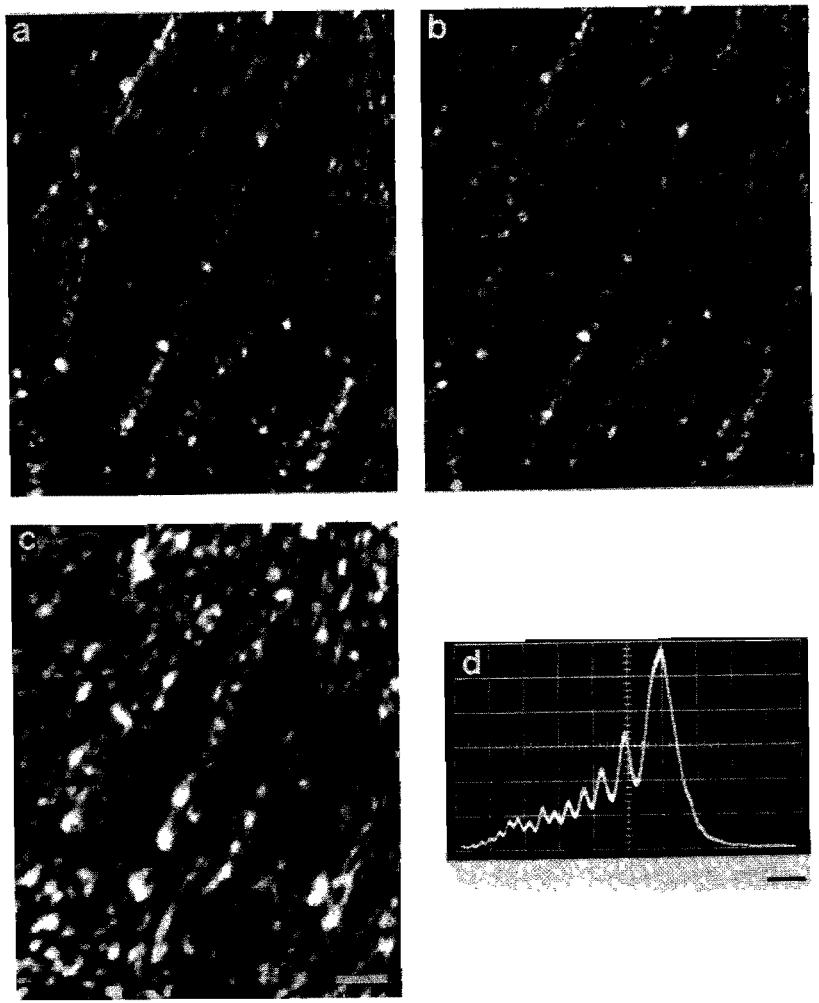

Figure 8.9. Changes in transverse resolution produced by varying the detector pinhole diameter or by introducing aberrations into the system. (a-c) Enlarged view of *Haemanthus* 15nm immunogold-labelled microtubule bundles using confocal reflected brightfield optics and a fluorite, N.A.=1.3 objective. (a) A 10 micron pinhole was placed in front of the detector. (b) Changing to a 2.5 micron detector pinhole shows an improvement in lateral resolution. Meaningful comparisons were made possible by measuring the background density and holding it constant during all steps in the photographic process. (c) Image of the same region using the same objective with its tube length correcting lens removed, i.e. the image plane (detector) is much farther away than the 160mm optimum tube length. Aberrations present in this configuration greatly reduce resolution. (d) $V(z)$ plot of this incorrect tube length condition in which side-lobes on the left side of the central peak result from spherical aberration effects of high numerical aperture. (a-c) Scale=2μm. (d) Horizontal scale=2μm in z.

10μm diameter pinhole in front of the detector. Changing to a 2.5μm detector pinhole, Figure 8.9(b), gives an improvement in lateral resolution which is in keeping with predictions based on theory [Wilson and Carlini, 1987]. On the other hand, Figure 8.9(c) shows the effects of using an objective that has not been precisely corrected for tube length. The microtubule bundles in the resulting image are virtually impossible to distinguish owing to the presence of spherical aberration, which is confirmed by the presence of multiple side peaks in the $V(z)$ plot in Figure 8.9(d).

It should be mentioned that all of these factors affect axial resolution as well, and in particular we have found that it is very sensitive to even small amounts of aberration.

III.2.3. Using detector arrays to further increase resolution

It is possible to further increase both the axial and transverse resolution of the confocal microscope by using a detector consisting of an array of rings [Sheppard and Cogswell, 1990]. One method for implementing this type of array detector configuration is to subtract an image formed using a somewhat larger detector pinhole from the image formed by a small pinhole (i.e. one that provides maximum resolution, as discussed in the previous section).

To illustrate this technique, experiments were conducted using our specimen-scanning confocal microscope and two photomultiplier detectors. A pinhole of 5μm diameter was placed in front of one detector and a 150μm diameter pinhole was positioned in front of the other. These were selected as being optimal for the 1.3 N.A. objective lens used in the system. Initially, $V(z)$ measurements were recorded for each detector using a front surface mirror as the sample. Following careful alignment of the two detector signals both in the axial as well as transverse directions, the amplitude of the signal from the detector having the larger pinhole was adjusted to be half that of the smaller. Subtracting this half-amplitude signal from that of the smaller pinhole produced a narrower central peak (improved axial resolution) in the resulting $V(z)$. This effect is illustrated at the top of Figure 8.10 where (A) was made using the 5μm detector pinhole, (B) was with the 150μm detector pinhole and (A-50%B) represents the first signal minus the second at half amplitude. To test for improvements in lateral resolution, the same system was used to observe 15nm immunogold-labelled microtubule bundles in a mitotic anaphase nucleus of *Haemanthus katherinae* endosperm (illustrated at the bottom of Figure 8.10). As one would expect, the resolution of fine structure is noticeably better in (A) as compared to (B). The image produced by using the difference signal (A-50%B) shows an even greater improvement

in transverse resolution, although at the expense of introducing some background noise. The axial resolution has also improved to the extent that it is difficult to see continuity along the strands of microtubule bundles, their resolution in depth being limited to a narrow plane.

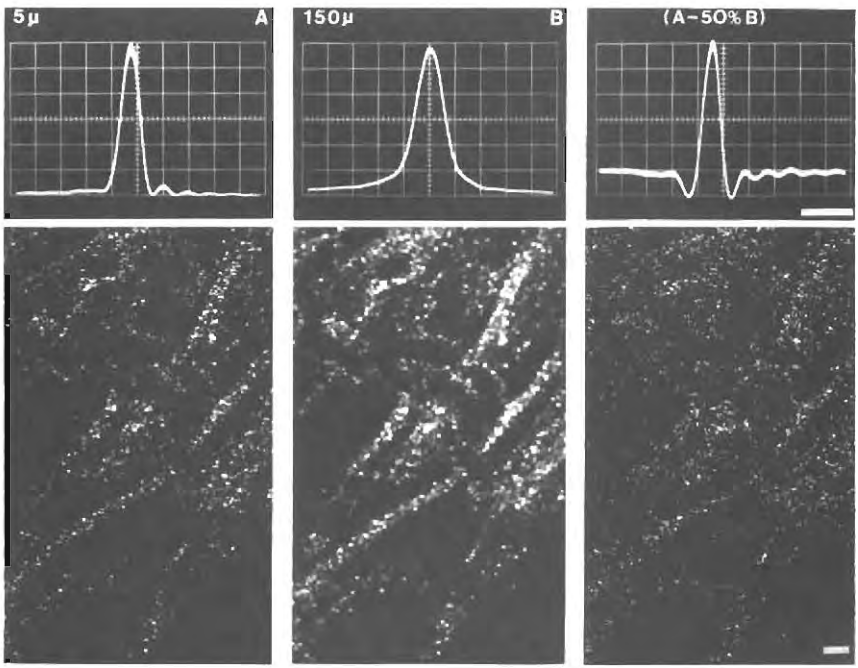

Figure 8.10. Improvement in lateral and axial resolution obtained from a confocal reflected brightfield configuration using two detectors. At the top of the figure are $V(z)$ plots showing the axial resolution response while at the bottom are actual images of an enlarged region of a mitotic metaphase in endosperm tissue of *Haemanthus katherinae*. Microtubule bundles have been labelled with 15nm immunogold. Objective was a fluorite 100X, N.A.=1.3. (A) Image formed with a 5μm diameter pinhole in front of one photomultiplier detector. (B) Image formed with a 150μm diameter pinhole in front of a second detector shows reduced resolution. (A-50%B) Image formed by subtracting a portion (50%) of the 150μm pinhole detector signal from the 5μm pinhole detector signal. This shows an increase in lateral resolution and such an improvement in axial resolution (optical sectioning) that it is now difficult, with just a single image, to see continuity along the microtubule strands. Horizontal scale=1μm. *Haemanthus* scale=2μm.

III.3. Improving visibility of image features by electronic differentiation

In the past decade, the development of digital image-processing and analysis techniques has had a strong impact in conventional and confocal microscopy. Although our microscope system commonly employs standard digital image-processing routines to enhance visibility of various specimen features, a description of these routines falls outside the scope of this chapter. However, it is probably worthwhile to

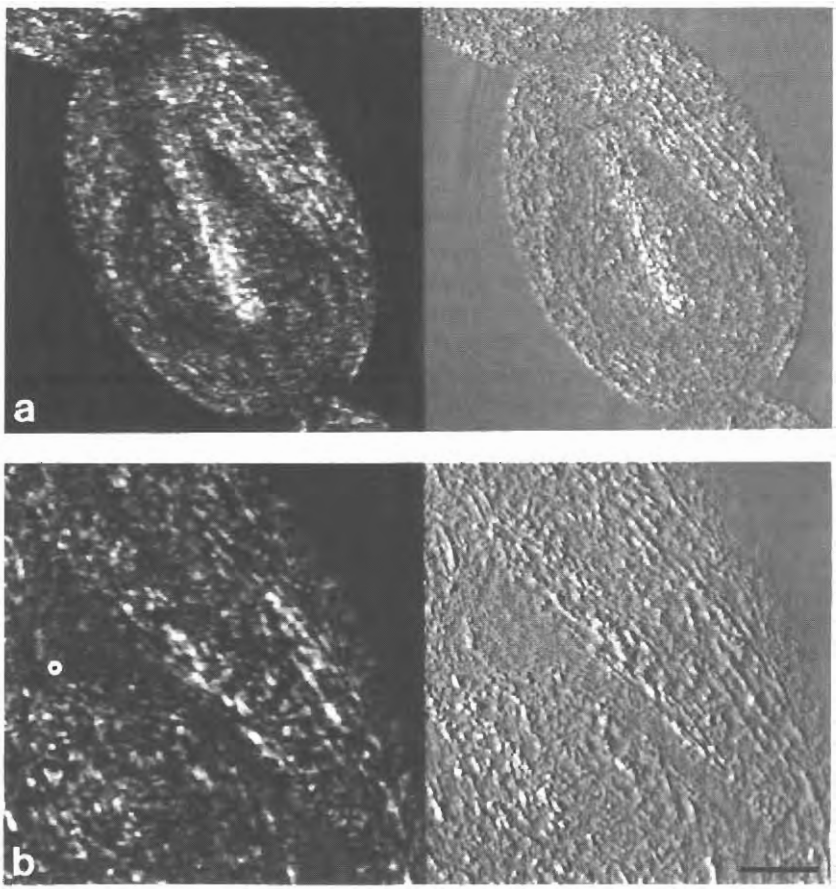

Figure 6.11. Use of electronic differentiation to enhance visibility of image detail. Subject is a living *Tradescantia* stamen hair cell mounted in water. (a) Shows an entire cell while (b) is an enlarged view of the upper right region, focused at the same plane (near the top surface). Left images are confocal reflected brightfield while right images have been electronically differentiated to reduce the distracting speckle appearance of the standard confocal configuration, thus making cell surface striations more visible to the observer. Scale=10μm.

briefly describe at this point a technique that we have used to improve the visual appearance of certain features in an image. This process electronically differentiates the analogue signal generated by the photomultiplier detector prior to its being digitized and displayed by the computer. Figures 8.11(a-b) show a low and a higher magnification view of a living *Tradescantia* stamen hair cell, with the left images made using the standard reflected confocal configuration and the right images produced by electronically differentiating the confocal analogue signal. This edge-enhancement technique was employed to assist the human observer in distinguishing meaningful cell surface structure (striations) from the speckle pattern that is commonly present in high magnification images produced using coherent (laser) illumination.

IV. Differential phase contrast

In a scanning microscope it is possible to include another extremely useful optical configuration which can produce non-confocal (increased depth of field) images in transmission at the same time as the confocal reflection images. This technique, called differential phase contrast (dpc), provides the opportunity for retrieval of information regarding slight changes in refractive index within a biological subject or between the subject and its surrounding medium. The system is able to detect refraction effects at edges (refractive index boundaries) which results in phase information being imaged in addition to the amplitude information (i.e. absorption) characteristic of conventional brightfield microscopes [Hamilton and Sheppard, 1984]. These refraction effects are dependent on the angle of incidence of the illuminating beam and the orientation of the edge (refractive index boundary) in the sample. Two images, each produced by an opposing half-aperture detector, will appear different wherever a component of an edge boundary parallel to the half-aperture division has produced a tilt in the resulting transmitted beams. When these two images are subtracted (and an offset midtone-grey signal added to improve visibility) the resulting image shows alternate highlights and shadows (in bas-relief) along refractive index boundaries.

In practice, we have found that simultaneously producing and displaying a differential phase contrast image of our biological subject while acquiring confocal reflection images gives an extremely useful frame of reference for locating otherwise indistinguishable internal features (such as nuclei, chromosomes, vacuoles, axons and cell bodies to name a few examples). Figure 8.7(a) shows an example of a transmitted dpc image of a *Haemanthus* anaphase which was produced at the same time as the confocal reflection images. The dpc technique

clearly shows the location of the chromosomes within the mitotic spindle which is composed of microtubule bundles.

The substage split detector used in transmitted differential phase contrast imaging can also be readily adapted to other useful configurations. For example, simply adding the two images from each side of the split detector gives a conventional transmitted brightfield image, Figure 8.12(c), as compared to the dpc image in Figure 8.12(d). Displaying the images from each half of the detector side-by-side gives a stereo pair brightfield image, Figures 8.12(a) and 8.12(b). This is similar to stereo pair-producing techniques used in conventional microscopy. The subject in this figure is a *Haemanthus* anaphase labelled with 5nm immunogold.

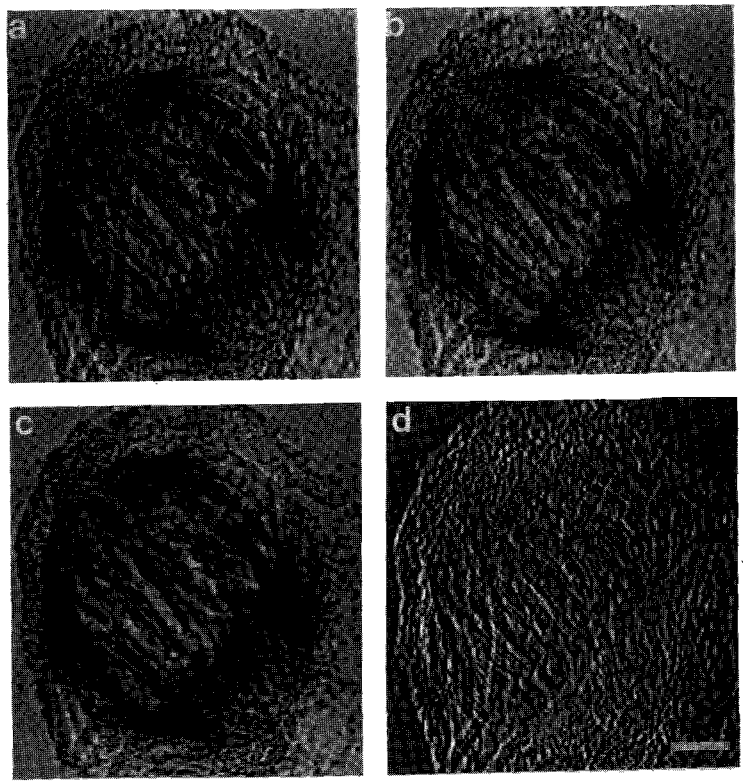

Figure 8.12. Non-confocal transmission images of a *Haemanthus* endosperm anaphase produced using a split detector in a variety of configurations. (a) and (b) are images from the left and right half of the split detector respectively which, when viewed together, form a stereo pair. (c) Transmitted brightfield image created by adding the signals from each half of the split detector. (d) Differential phase contrast image produced by subtracting the signal in (b) from that in (a) and adding an offset grey. Scale=5μm.

clearly shows the location of the chromosomes within the mitotic spindle which is composed of microtubule bundles.

The substage split detector used in transmitted differential phase contrast imaging can also be readily adapted to other useful configurations. For example, simply adding the two images from each side of the split detector gives a conventional transmitted brightfield image, Figure 8.12(c), as compared to the dpc image in Figure 8.12(d). Displaying the images from each half of the detector side-by-side gives a stereo pair brightfield image, Figures 8.12(a) and 8.12(b). This is similar to stereo pair-producing techniques used in conventional microscopy. The subject in this figure is a *Haemanthus* anaphase labelled with 5nm immunogold.

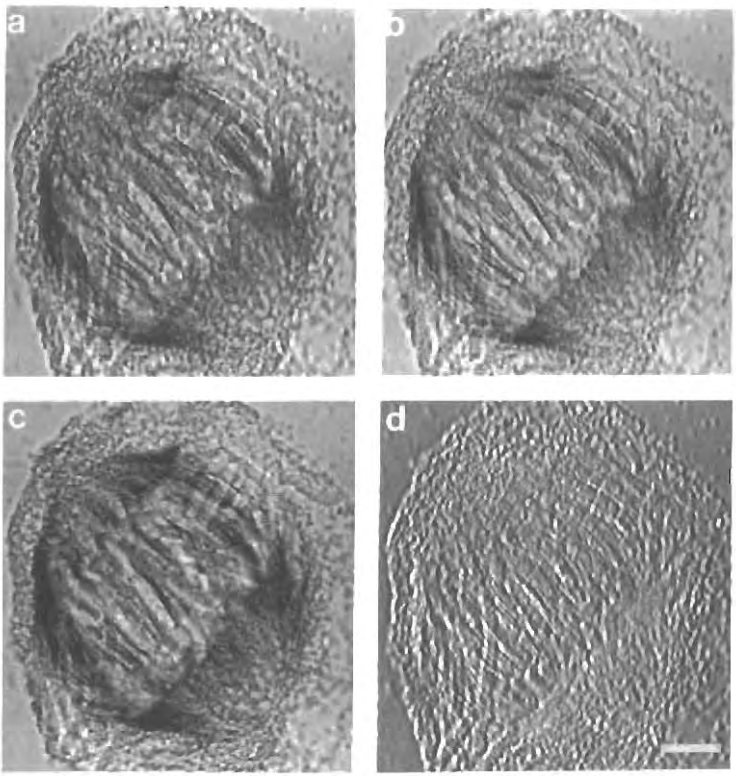

Figure 8.12. Non-confocal transmission images of a *Haemanthus* endosperm anaphase produced using a split detector in a variety of configurations. (a) and (b) are images from the left and right half of the split detector respectively which, when viewed together, form a stereo pair. (c) Transmitted brightfield image created by adding the signals from each half of the split detector. (d) Differential phase contrast image produced by subtracting the signal in (b) from that in (a) and adding an offset grey. Scale=5μm.

It is even possible to produce usable stereo pairs from a through-focus series in differential phase contrast if a high numerical aperture condenser (collector) lens is used between the specimen and the split detector to produce images of reasonably high axial resolution (ca. 1μm). This technique was employed to produce a stereo pair image of a portion of a living *Tradescantia* stamen hair cell, mounted in water between two sealed coverglasses, Figure 8.13. Even though the six dpc images used to create the stereo pair are not confocal, the axial resolution is good enough to produce a clear indication of the location of the cell nucleus and surface striations in depth.

Finally, it is possible to enhance or subdue specific spatial frequencies in differential phase contrast images by using a variety of detector aperture masks [Hamilton *et al.*, 1984].

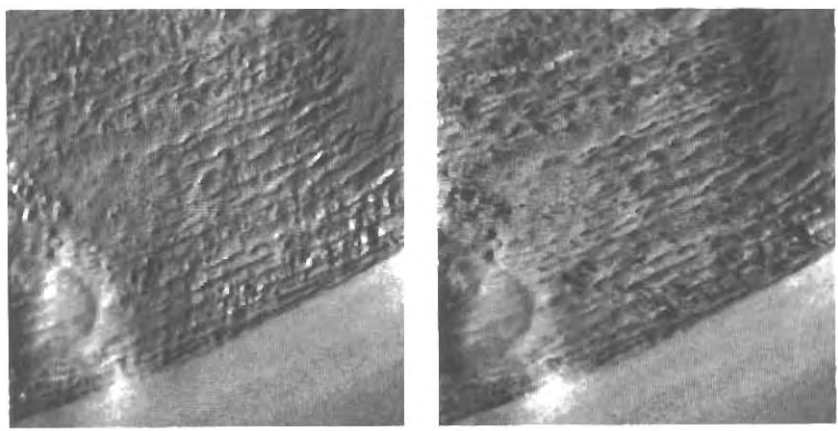

Figure 8.13. Stereo pair produced from a series of 6 ***non-confocal*** transmitted differential phase contrast images at 0.4μm focus intervals. Subject is a portion of a living *Tradescantia* stamen hair cell, mounted in water between two coverglasses. High numerical aperture immersion objectives (N.A.=1.3 and 1.25) were used above and below the sample to improve the resolution of the transmitted dpc images. Scale=5μm.

V. Confocal transmission

Interestingly, confocal microscopy in the transmission mode, although available for some time [Brakenhoff *et al.*, 1979; Sheppard and Wilson, 1979], has received little attention in recent years, perhaps because of difficulties in aligning the optical system and maintaining its alignment during scanning. Confocal transmission microscopy does not exhibit as strong an optical sectioning property as in the reflection mode [Sheppard, 1986] but, combined with the facility for electronic contrast

It is even possible to produce usable stereo pairs from a through-focus series in differential phase contrast if a high numerical aperture condenser (collector) lens is used between the specimen and the split detector to produce images of reasonably high axial resolution (ca. 1μm). This technique was employed to produce a stereo pair image of a portion of a living *Tradescantia* stamen hair cell, mounted in water between two sealed coverglasses, Figure 8.13. Even though the six dpc images used to create the stereo pair are not confocal, the axial resolution is good enough to produce a clear indication of the location of the cell nucleus and surface striations in depth.

Finally, it is possible to enhance or subdue specific spatial frequencies in differential phase contrast images by using a variety of detector aperture masks [Hamilton *et al.*, 1984].

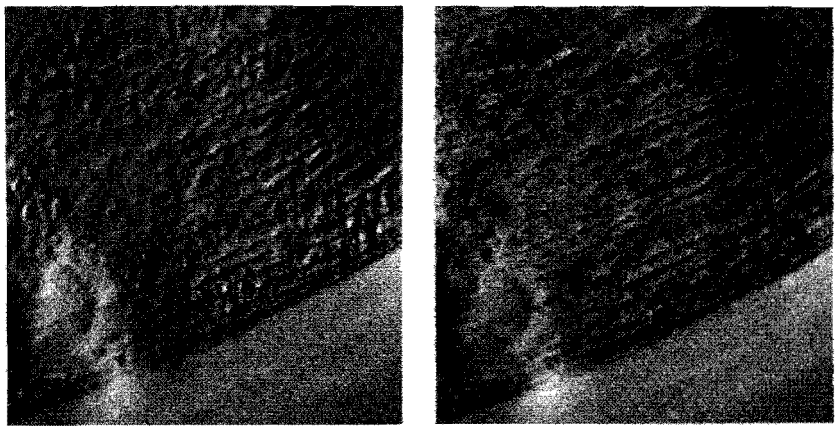

Figure 8.13. Stereo pair produced from a series of 6 *non-confocal* transmitted differential phase contrast images at 0.4μm focus intervals. Subject is a portion of a living *Tradescantia* stamen hair cell, mounted in water between two coverglasses. High numerical aperture immersion objectives (N.A.=1.3 and 1.25) were used above and below the sample to improve the resolution of the transmitted dpc images. Scale=5μm.

V. Confocal transmission

Interestingly, confocal microscopy in the transmission mode, although available for some time [Brakenhoff *et al.*, 1979; Sheppard and Wilson, 1979], has received little attention in recent years, perhaps because of difficulties in aligning the optical system and maintaining its alignment during scanning. Confocal transmission microscopy does not exhibit as strong an optical sectioning property as in the reflection mode [Sheppard, 1986] but, combined with the facility for electronic contrast

enhancement, it can result in useful information. The alignment problem stems from the fact that refractive index inhomogeneities cause the transmitted beam to move in the plane of the pinhole. Although it could be argued that the resultant variations in signal provide meaningful information, nevertheless it is difficult to maintain an adequate signal and be sure that the system is correctly aligned. This problem can be alleviated by reflecting the transmitted light back through the object with a phase conjugate mirror [Cathey *et al.*, 1986]; however, some improvement can be obtained simply by reflecting the light with an ordinary mirror. The light transmitted through the object for the first time is focused onto a mirror and refocussed back onto the object. In this case, lateral movements of the transmitted light spot are cancelled on the return path, but not axial movements. This double-pass method was described by Sheppard and Wilson (1980) and is commercially available on the Lasertec microscope. We have used this technique with a pair of high aperture oil immersion objectives and a sample mounted between coverslips to avoid the introduction of unwanted spherical aberration. Figure 8.14 shows three stereo pair images of a *Tradescantia* stamen hair cell. Figure 8.14(a) shows a confocal reflected brightfield image which clearly delineates the surface striations in the cell wall. (This image is actually a projection of several planes of focus produced by using the auto-focus technique in which the maximum signal is retained during scanning.) The double-pass confocal transmission image of Figure 8.14(b) shows the cell nucleus and is again a projection, but this time generated by retaining the minimum signal. Figure 8.14(c) shows a double-pass confocal transmission differential phase contrast image, formed by using two detectors with a half-plane mask in the lens pupil. This method [Benschop, 1987] gives differential phase contrast in reflection from surfaces while also exhibiting confocal optical sectioning. We have found that analogous images in reflection from semi-transparent objects are difficult to interpret, as confocal reflection always gives differential contrast from axial variations in refractive index, and this results in a complicated behaviour when combined with half-plane apertures. However, these problems are overcome in confocal transmission and phase information is imaged.

VI. Confocal differential interference contrast (DIC)

The Nomarski DIC method [Nomarski, 1955] can be used in reflection in a confocal microscope and is especially suited to imaging subjects having strongly reflecting surface topographies with underlying opaque regions similar to the types of specimens described earlier in this chapter. The DIC optics provide surface texture information in

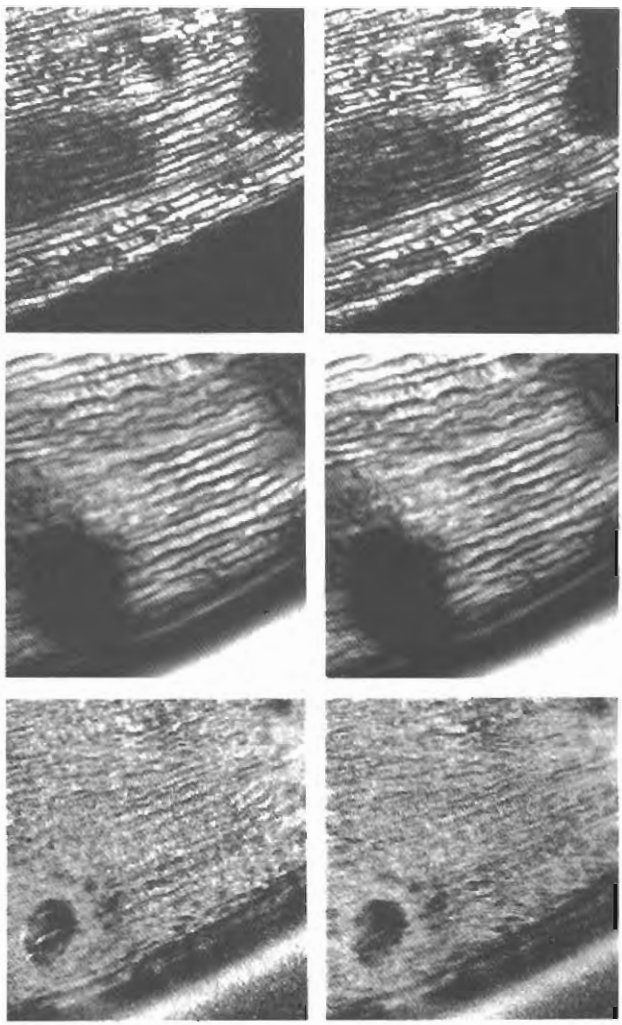

Figure 8.14. Stereo pairs produced using *confocal* double-pass transmission techniques both for brightfield and differential phase contrast imaging. Subject and objectives are the same as in Figure 8.13. (a) Confocal reflected brightfield (included here for comparison) shows surface striations in the *Tradescantia* stamen hair cell wall from 4 planes of focus at 0.2μm steps. (b) Double-pass confocal transmission from 4 planes of focus at 0.4μm steps shows the location of the cell nucleus in the lower left region, in addition to surface structure. (c) Double-pass transmission with two detectors and half-plane masks in the lens pupil gives confocal differential phase contrast (created from 8 planes at 0.2μm steps). This technique more clearly delineates the nucleus and shows surface striations in bas-relief. Scale same as Figure 8.13.

bas-relief, which is superimposed on the already strong optical sectioning property of confocal reflection. Figures 8.15(a) and 8.15(b) show a comparison of the brightfield and DIC techniques using a commercially manufactured integrated circuit as a subject. The images were created using the auto-focus technique over 5 planes of focus at 0.4μm steps. To obtain DIC, a Nomarski-modified Wollaston prism was inserted above the rear pupil of the objective and an analyser placed in the reflected beam before the detector converging lens. As always, the on-axis design of our system allows the use of full-aperture, high N.A. optics at any magnification. This provides high axial resolution and thereby limits the bas-relief information characteristic of DIC to being within the depth of the currently resolved optical section.

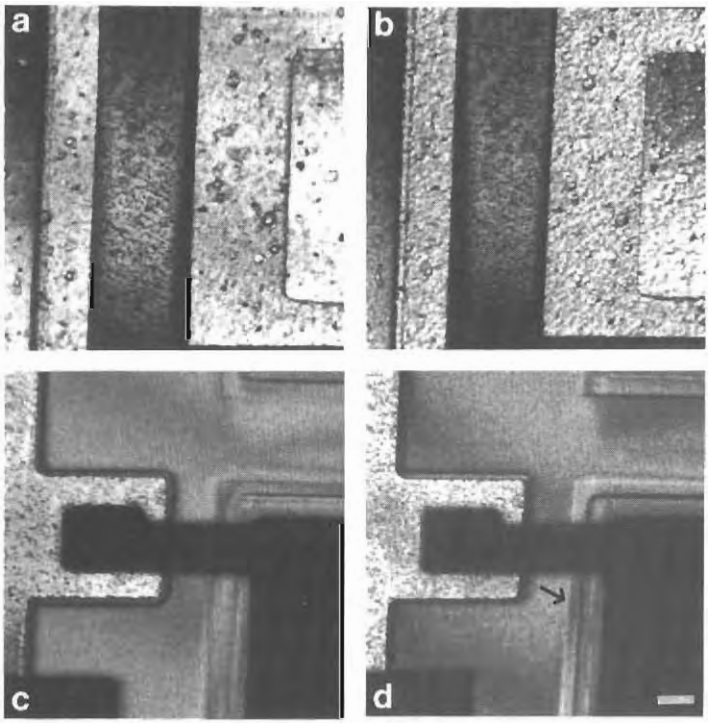

Figure 8.15. Comparison of images created using confocal reflected brightfield versus confocal reflected Nomarski DIC techniques. Subject is a portion of a commercially manufactured integrated circuit. Objective is oil immersion, N.A.=1.3. (a-b) Auto-focus images from 5 planes, created using brightfield (a) and Nomarski optics (b), show the increased delineation of surface roughness due to the bas-relief effects of Nomarski. (c-d) Brightfield versus Nomarski auto-focus images of a different region of the sample show an improvement in the ability of the DIC technique (d) to accurately delineate phase edges (i.e. small changes in surface height denoted by arrow). Scale=10μm.

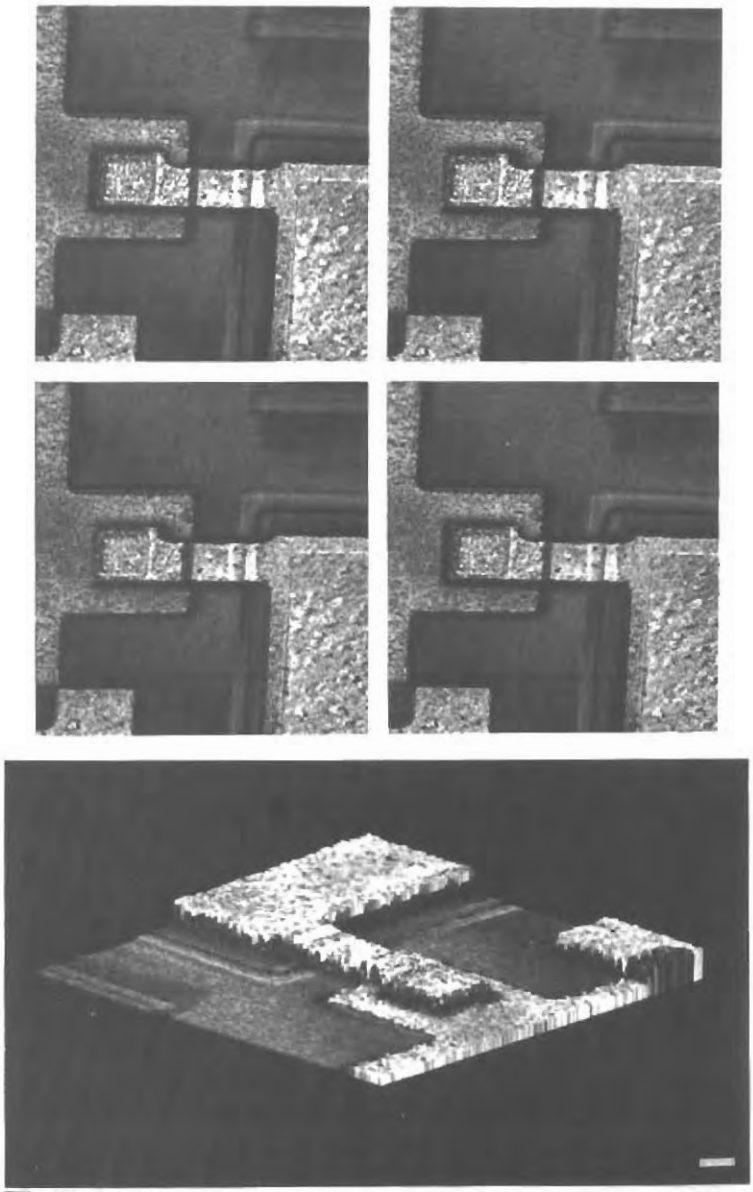

Figure 8.16. Confocal reflected Nomarski DIC of an integrated circuit using an N.A.=1.3, oil immersion objective. (Top) Stereo pair (for normal viewing) created by storing the brightest signal from 12 successive planes in a through-focus series at 0.5μm focus steps. This technique shows fine structure of surfaces in bas-relief at successive planes of focus. (Middle) Same stereo pair as above but arranged for viewing with crossed eyes. (Bottom) An isometric projection of the same 12 images showing surface details and height information. Scale=10μm.

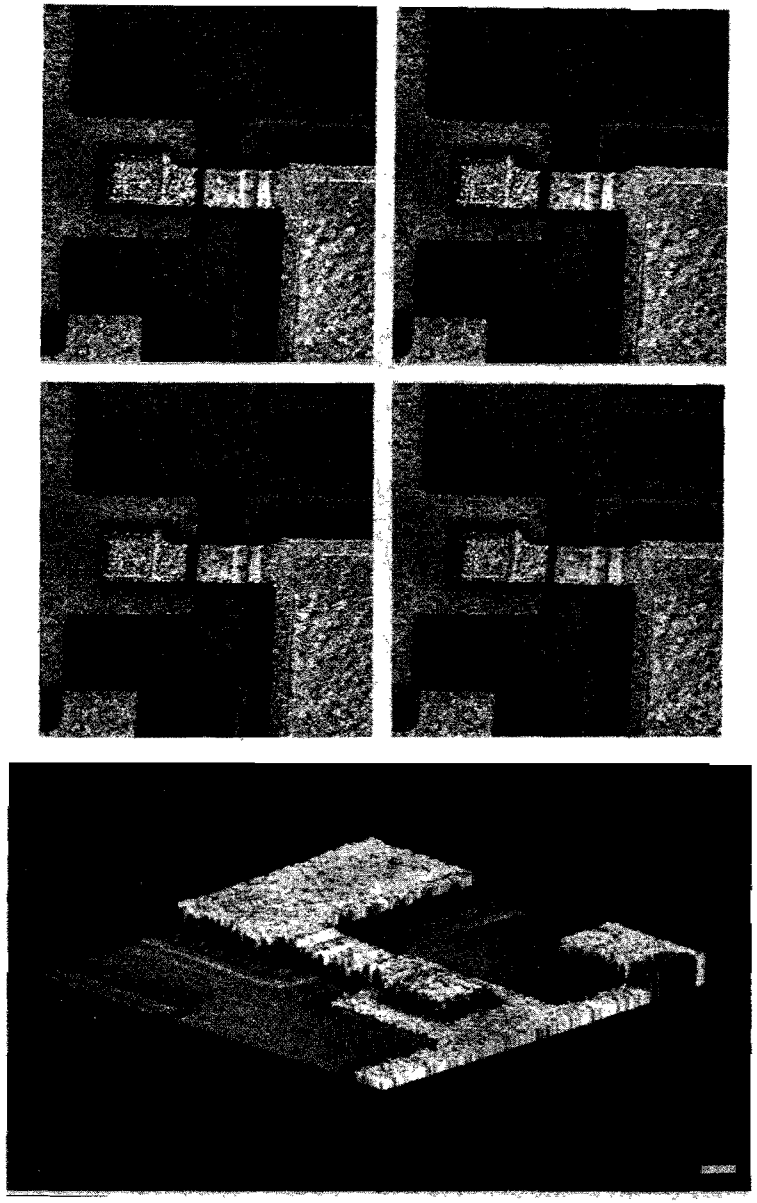

Figure 8.16. Confocal reflected Nomarski DIC of an integrated circuit using an N.A.=1.3, oil immersion objective. (Top) Stereo pair (for normal viewing) created by storing the brightest signal from 12 successive planes in a through-focus series at 0.5μm focus steps. This technique shows fine structure of surfaces in bas-relief at successive planes of focus. (Middle) Same stereo pair as above but arranged for viewing with crossed eyes. (Bottom) An isometric projection of the same 12 images showing surface details and height information. Scale=10μm.

In addition to enhancing surface texture, we have found that the use of DIC avoids problems in interpretation of images from phase objects which may be caused, for example, by small surface-height changes. Figures 8.15(c) and 8.15(d) show another region of the same integrated circuit focused on a shallow-ridged structure just above the base substrate. The reflected Nomarski image clearly delineates the ridge-groove morphology which is distorted in the brightfield image.

In order to demonstrate the potential of DIC for producing three-dimensional images with well-delineated phase edges and surface fine-structure, a series of 12 images at 0.5μm focus steps was used to form an auto-focus image starting at the top of the same region of the sample, Figure 8.16 (top left). There is no problem in utilizing the auto-focus method since DIC gives a combination of differential phase and amplitude information. Therefore, it is not necessary to add a midtone-grey offset to the displayed image, as in the differential phase method with half-plane apertures described earlier. In Figure 8.16 (top right) the same imaging technique was used but with images from successive planes of focus displaced laterally by one pixel to produce a stereo pair. Figure 8.16 (bottom) shows a computer reconstruction of an isometric projection (looking across the sample from the upper left corner) which was formed using the differential interference contrast images.

Although the confocal reflected Nomarski technique has been illustrated here using a highly reflective metallic subject, one can conceive of many potential applications in the biological sciences: for example, imaging surfaces of seeds, spores and pollen grains.

VII. Conclusion

In this chapter we have attempted to show that, with an on-axis scanning microscope, a range of brightfield configurations is possible with all the advantages inherent in a confocal design. These have the potential for providing new and extremely useful information especially in applications using living or freshly prepared tissue, immunogold and silver probes, naturally pigmented or differentially stained material, or subjects with highly reflective surface topography. The microscopist must not assume, however, that conventional methods of biological sample preparation or even high quality conventional microscope objectives will perform in predictable ways on a confocal instrument — careful consideration of how the image is formed and what is being imaged is paramount in correct usage of the system and accurate interpretation of the results. Therefore, for these techniques to find widespread usage in the biological sciences, continued improvements in confocal optical instrumentation must proceed in tandem with new

developments in sample preparation in order for clearly understandable images to be generated.

Acknowledgements

This work was performed while the authors were at the Department of Engineering Science, University of Oxford. We wish to thank D.K. Hamilton, University of Oxford, for frequent input and assistance with the experiments and instrumentation. We thank the Plant Anatomy and the Cytology Departments, Royal Botanic Gardens, Kew, for the loan of plant specimens. We also wish to express our appreciation to A.S. and J.M. Bajer and J. Karpilow for providing biological samples, H.M. Howard and S.A. Poston for photographic assistance and D.E. Wimber, University of Oregon for editorial comments.

References

Benschop, J. P. H., (1987). Confocal differential phase contrast in scanning optical microscopy. Proc. S.P.I.E., **809**, 90-96.

Born, M. and Wolf, E., (1980). *Principles of optics.* pp. 661. Pergamon Press, Oxford.

Brakenhoff, G. J., Blom, P. and Barends, P., (1979). Confocal scanning light microscopy with high aperture immersion lenses. J. Microsc., **117**, 219-232.

Carlsson, K., Danielsson, P. E., Lenz, R., Liljeborg, A., Majlöf, L. and Åslund, N., (1985). Three-dimensional microscopy using a confocal laser scanning microscope. Opt. Lett., **10**, 53-55.

Cathey, W. T., Johnson, K. M. and Cormack, R. H., (1986). Phase conjugate resonator for high-resolution scanning microscopy. J. Opt. Soc. Am., **A3**, P24.

Cogswell, C. J., Sheppard, C. J. R., Moss, M. C. and Howard, C. V., (1990). A method for evaluating microscope objectives to optimize performance of confocal systems. J. Microsc. To be published.

Hamilton, D. K. and Sheppard, C. J. R., (1984). Differential phase contrast in scanning optical microscopy. J. Microsc., **133**, 27-39.

Hamilton, D. K., Sheppard, C. J. R. and Wilson, T., (1984). Improved imaging of phase gradients in scanning optical microscopy. J. Microsc., **135**, 275-286.

Inoué, S., (1989). Foundations of confocal scanned imaging in light microscopy. In: *The handbook of biological confocal microscopy.* Pawley, J. (Editor), 1-13. I.M.R. Press, Madison, Wisconsin.

Nomarski, G., (1955). Microinterferometrie differential a ondes polarisées. J. Phys. Radium, **16**, 9-135.

Sheppard, C. J. R., (1977). The scanning optical microscope. I.E.E.E. J. Quantum Elec., **QE-13**, 100D.

Sheppard, C. J. R., (1986). The spatial frequency cut-off in three-dimensional imaging II. Optik, **74**, 128-129.

Sheppard, C. J. R. and Choudhury, A., (1977). Image formation in the scanning microscope. Opt. Acta, **24**, 1051-1073.

Sheppard, C. J. R. and Cogswell, C. J., (1990). Confocal microscopy with detector arrays. J. Modern Opt. To be published.

Sheppard, C. J. R. and Wilson, T., (1979). Effect of spherical aberration on the imaging properties of scanning optical microscopes. Appl. Opt., **18**, 1058-1063.

Sheppard, C. J. R. and Wilson, T., (1980). Multiple traversing of the object in the scanning microscope. Opt. Acta, **27**, 611-624.

Wilson, T. and Carlini, A. R., (1987). Size of the detector in confocal imaging systems. Opt. Lett., **12**, 227-229.